Bioorganic & Medicinal Chemistry 17 (2009) 4367–4377

Contents lists available at ScienceDirect

Bioorganic & Medicinal Chemistry

journal homepage: www.elsevier.com/locate/bmc

Synthesis and biological evaluation of novel carbon-11 labeled pyridyl ethers: candidate ligands for in vivo imaging of α4β2 nicotinic acetylcholine receptors (α4β2-nAChRs) in the brain with positron emission tomography

Yongjun Gao [a], Hayden T. Ravert [a], Hiroto Kuwabara [a], Yingxian Xiao [b], Christopher J. Endres [c], John Hilton [a], Daniel P. Holt [a], Anil Kumar [a], Mohab Alexander [a], Dean F. Wong [a], Robert F. Dannals [a], Andrew G. Horti [a,*]

[a] PET Center, Division of Nuclear Medicine, Department of Radiology, The Johns Hopkins University School of Medicine, 600 North Wolfe Street, Nelson B1-122, Baltimore, MD 21287-0816, USA
[b] Department of Pharmacology, Georgetown University, 3900 Reservoir Road, NW Washington, DC 20057, USA
[c] Division of Neuroradiology, Department of Radiology, The Johns Hopkins University School of Medicine, 600 North Wolfe Street, Baltimore, MD 21287-0816, USA

ARTICLE INFO

Article history:
Received 17 March 2009
Revised 5 May 2009
Accepted 9 May 2009
Available online 15 May 2009

Keywords:
Nicotinic acetylcholine receptor
nAChR
PET
Radioligand

ABSTRACT

The most abundant subtype of cerebral nicotinic acetylcholine receptors (nAChR), α4β2, plays a critical role in various brain functions and pathological states. Imaging agents suitable for visualization and quantification of α4β2 nAChRs by positron emission tomography (PET) would present unique opportunities to define the function and pharmacology of the nAChRs in the living human brain. In this study, we report the synthesis, nAChR binding affinity, and pharmacological properties of several novel 3-pyridyl ether compounds. Most of these derivatives displayed a high affinity to the nAChR and a high subtype selectivity for α4β2-nAChR. Three of these novel nAChR ligands were radiolabeled with the positron-emitting isotope ^{11}C and evaluated in animal studies as potential PET radiotracers for imaging of cerebral nAChRs with improved brain kinetics.

1. Introduction

Nicotinic acetylcholine receptors (nAChRs) are pentameric ligand-gated ion channels that are formed by combinations of various α and β subunits. The subunit combinations define different receptor subtypes with distinct biophysical, physiological and pharmaceutical properties as well as different locations throughout the nervous systems.[1–4] Many studies have shown that nAChRs could play important roles in brain functions and are also involved in various brain pathologies such as Alzheimer's disease, Parkinson's disease, schizophrenia, anxiety, and nicotine addiction.[5–8]

The in vivo imaging of nAChRs with positron emission tomography (PET) promises to improve our understanding of various CNS disorders. During the last decade there has been considerable interest in the development of suitable PET radioligands for imaging nAChRs, in particular, the most abundant α4β2-nAChR subtype. The current development of nAChR PET radioligands has mostly focused on the analogs of (*S*)-3-(1-methylpyrrolidin-2-yl)pyridine (nicotine, **1**) and 2-(6-chloro-3-pyridinyl)-7-azabicyclo[2.2.1]heptane (epibatidine, **2**) and, more recently, on a series of compounds that were developed by Abbott Laboratories, including (*S*)-3-(azetidin-2-ylmethoxy)pyridine (A-85380, **3**) and (*S*)-3-((1-methylpyrrolidin-2-yl)methoxy)pyridine (A-84543, **4**) (Fig. 1).[9,10]

The interested reader will be able to find more details on the development of these nAChR PET radioligands in several recent reviews.[11–18]

Presently, only two radiotracers, 2-[^{18}F]fluoro-A-85380 (**5**), and 6-[^{18}F]fluoro-A-85380 (**6**) (Fig. 2), are available for studying α4β2 nAChRs in human brain using PET.[19–25] The slow brain kinetics of these radiotracers hamper quantification of the nAChR since it takes 4–7 h of PET scanning for the tracer radioactivity to reach a

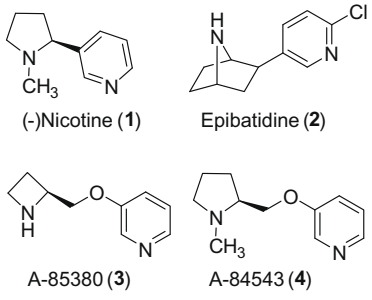

Figure 1. Representative nAChR ligands—main lead compounds for development of nAChR PET radioligands.

* Corresponding author. Tel.: +1 410 614 5130.
E-mail address: ahorti1@jhmi.edu (A.G. Horti).

0968-0896/$ - see front matter © 2009 Elsevier Ltd. All rights reserved.
doi:10.1016/j.bmc.2009.05.021

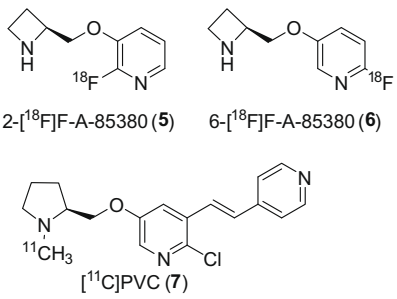

Figure 2. Radiolabeled 3-pyridyl ether compounds as PET radiotracers for imaging nAChR.

spatial-temporal steady state.[11] The most recent review about the nAChR PET radioligands[26] describes several analogs of **5** with improved brain kinetics, but the combined imaging properties of these radiolabeled A-85380 analogs in animals were not sufficiently promising for human studies.

Previously, we developed [^{11}C]CH_3-PVC (**7**),[27–29] (Fig. 2) a radiolabeled analog of A-84543 (**4**) with faster kinetics in the Rhesus monkey brain than those of **5** and **6**. The accelerated brain kinetics of **7** are thought to be associated with its higher lipophilicity and, consequently, better blood–brain barrier (BBB) permeability. However, the binding potential of **7** in Rhesus monkey brain was not sufficiently high for use in human subjects. We suggested that compounds that are structurally similar to **7,** and with similar lipophilicity but with a higher binding affinity, would display better imaging properties. We now report the synthesis, in vitro characterization, radiosynthesis, in vivo regional brain distribution in rodents and PET imaging in nonhuman primates of several novel analogs of **7** with improved imaging properties.

2. Results and discussion

2.1. Chemistry

Schemes 1 and 2 outline the synthesis of **16** and **25**. All novel compounds were characterized by ^{1}H NMR, MS, and elemental analysis prior to biological evaluation. The key intermediates **14, 23a** and **23b** were obtained by Mitsunobu reaction. The final *N*-methyl derivative **16** was prepared by deprotection of **14** with TFA followed by N-methylation with 37% HCHO/$NaBH_3CN$. Compounds **25a** and **25b** were obtained by heating of **23a** and **23b** with 37% HCHO/HCOOH.

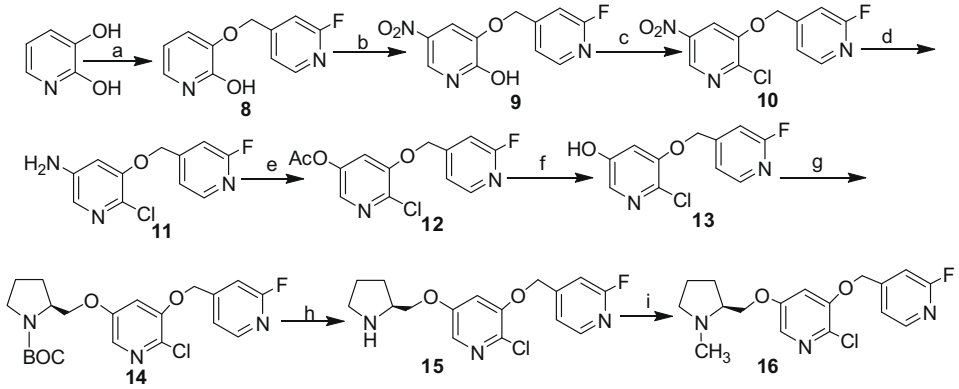

Scheme 1. Reagents: (a) NaOH, 4-bromomethyl-2-fluoropyridine, MeOH; (b) HNO_3/H_2SO_4; (c) $POCl_3$, quinoline; (d) Fe, H_2O, AcOH; (e) HBF_4, $NaNO_2/H_2O$; then Ac_2O; (f) 1 M KOH, MeOH; (g) DEAD, PPh_3, THF; (h) CF_3COOH/CH_2Cl_2; (i) aqueous $HCHO/NaBH_3CN$.

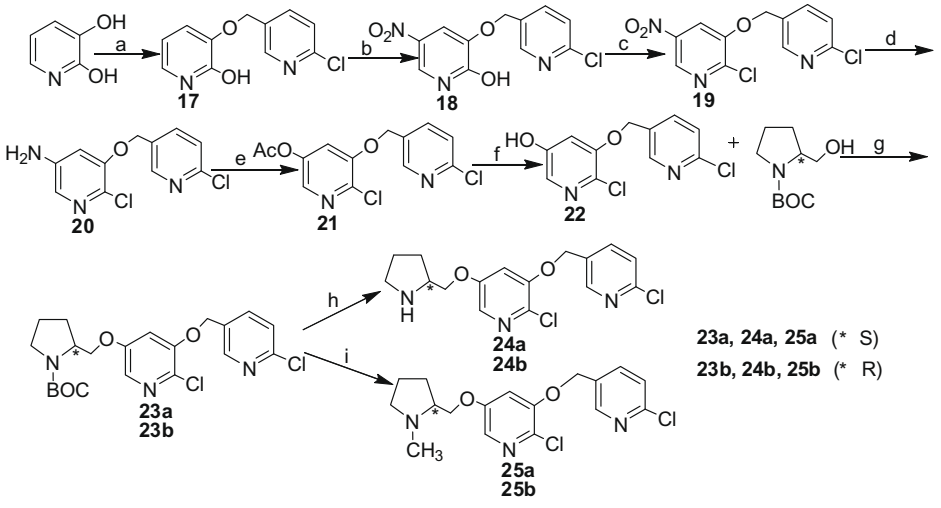

Scheme 2. Reagents: (a) NaOH, 2-chloro-5-(chloromethyl)pyridine, MeOH; (b) HNO_3/H_2SO_4; (c) $POCl_3$, quinoline; (d) Fe, H_2O, AcOH; (e) HBF_4, $NaNO_2/H_2O$, Ac_2O; (f) 1 M KOH, MeOH; (g) DEAD, PPh_3, THF; (h) CF_3COOH/CH_2Cl_2; (i) aqueous HCHO, HCOOH.

2.2. Lipophilicity

The partition coefficient between octanol and phosphate buffer at pH 7.4 (log $D_{7.4}$) of compounds **16, 25** and the previously described **26** ((*S*)-2-chloro-2′-fluoro-5-((1-methylpyrrolidin-2-yl)-methoxy)-3,4′-bipyridine)[30] were determined by a conventional shake-flask method (Table 1). These lipophilicity values correspond to an optimal range (1.5–3) for the most known PET radiotracers.[31]

2.3. Structure–binding affinity relationship

Our previous studies demonstrated that [^{11}C]Me-PVC (**7**)[29] (Fig. 2), a radiolabeled analog of A-84543 (**4**), exhibited substantially more rapid brain kinetics than those of 2-[^{18}F]fluoro-A-85380, the only available radioligand for imaging of nAChR in the human brain, which required 6–8 h of PET scanning due to its slow brain kinetics. Despite the optimized brain kinetics [^{11}C]Me-PVC (**7**) was not a good candidate for human studies because of its relatively low binding potential.[30] We hypothesized that an analog of **7** with higher binding affinity to α4β2 nAChRs might exhibit a higher binding potential while its brain kinetics remains sufficiently rapid. One of the important molecular properties of Me-PVC (**7**) is high conformational flexibility.[28] We hypothesized that replacement of the vinyl linker between the two pyridine rings with the more flexible-CH_2–O-linker could potentially enhance the binding affinity. This hypothesis was a driving force for the synthesis of the diether series **15**, **16** (Scheme 1) and **24** and **25** (Scheme 2), the analogs of **7** with improved conformational flexibility.

Binding affinities of all new nAChR ligands were determined in competition binding experiments using stably expressed transfected cell lines (α2β2-, α2β4-, α3β2-, α3β4-, α4β2- and α4β4-nAChR subtypes)[32] and the radioligand [^{3}H]epibatidine (Table 1). Subtype selectivity is a critical issue for the effectiveness and safety of nAChR ligands. α4β2 subtype and α3β4 subtype represent the main ganglionic nAChR population. The α3β4 subtype is found in many sympathetic ganglia, while the α4β2 subtype is the predominant nAChR in the forebrain; therefore, the affinity ratios of ligands at these subtypes can help to predict the likelihood of autonomic nervous system side effects of ligands aimed at the predominant receptor subtype in the forebrain. Thus we compared the affinities of these ligands at the α3β4 subtype with their affinities at the α4β2 subtype. The binding affinities of **16** and **25a** are very high and comparable with the binding affinity of epibatidine (Table 1). The previously synthesized ligand **26** (Fig. 7)[30] that does not have a linker between two pyridine rings showed similar binding affinity but its α4β2/α3β4 selectivity was greater than the selectivity of **16** and **25a**. Comparison of the α4β2-nAChR binding affinity of more rigid **26** with more flexible **16** and **25a** suggests that molecular flexibility within this series is not crucial parameter. The *R*-enantiomer **25b** showed substantially lower binding affinity at the α2β2 and α4β2 subtypes than the *S*-enantiomer **25a**.

2.4. Radiochemistry

Compounds **16**, **25a** and **26** were selected for further radiolabeling and animal studies because they exhibited the highest binding affinity at α4β2-nAChR within the series. Although compound **24a** displayed even higher binding affinity at α4β2-nAChRs than compounds **16**, **25a** and **26**, it was not further studied as radioligand owe to the lack of methyl group making ^{11}C-labeling difficult.

The straightforward preparation of [^{11}C]**16** and [^{11}C]**25a** was accomplished via N-methylation of the nor-methyl precursors **15** and **24a** with the [^{11}C]CH_3I in *N,N*-dimethylformamide as shown in Scheme 3. The final products [^{11}C]**16** and [^{11}C]**25a** were prepared in high radiochemical yield ([^{11}C]**16**—18.4 ± 8.8% (n = 4), [^{11}C]**25a**—29 ± 7.2% (n = 3)). The radiochemical purity was greater than 98% and specific radioactivity were: 8022 ± 5592 (n = 4) mCi/μmol for [^{11}C]**16** and 3646 ± 1233 mCi/μmol (n = 3) for [^{11}C]**25a** (nondecay corrected from the end of ^{11}CH_3I synthesis).

2.5. In vivo studies

The novel radioligands [^{11}C]**16**, [^{11}C]**25a** and the previously synthesized [^{11}C]**26** (Fig. 7)[30] were studied in rodents and baboon as potential probes for PET imaging of central nAChR.

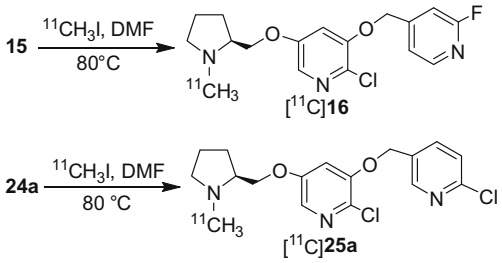

Scheme 3. Radiosynthesis of [^{11}C]**16** and [^{11}C]**25a**.

Table 1
Comparison of lipophilicity and binding affinities of (−)-nicotine, (±)epibatidine, 2-F-A-85380, **7** and new 3-pyridyl ether compounds **15**, **16**, **24a**, **25a**, **25b** and **26**

Compound	log $D_{7.4}$[a]	K_i, nM (defined rat nAChR subtypes)[b]						Selectivity α3β4/α4β2 (K_i ratio)
		α2β2	α2β4	α3β2	α3β4	α4β2 (K_{rel}[c])	α4β4	
(−)-Nicotine		12	110	47	440	10	40	44
(±)-Epibatidine		0.025	0.095	0.035	0.57	0.061	0.16	9
7	1.6[19]	—	—	—	—	0.028[d] (2.8)	—	—
5	−1.43[11]	1.4	180	3.0	3700	1.3 (21)	190	2846
15	1.4	0.035	8.2	0.25	43	0.13 (2.1)	1.1	331
16	1.8	0.022	11	0.33	90	0.062 (1.0)	1.6	1452
24a	1.9	0.0056	4.1	0.041	79	0.028 (0.5)	0.49	2821
25a	2.2	0.031	14	0.26	320	0.055 (0.9)	6.6	5818
25b	2.2	1.5	22	0.85	350	1.1 (18.0)	7.6	318
26	1.6	0.050	27	0.71	590	0.062 (1.0)	16	9516

[a] The partition coefficient between octanol and water at pH 7.4 was measured as described previously.[30]
[b] Competitive binding experiments were conducted as described previously.[32] K_i values of (−)-nicotine and (±)-epibatidine were taken from the literature,[32,33] and are shown here for comparison. The K_i values shown were calculated from competition bindings with 10 concentrations of the tested ligands (**5**, **15**, **16**, **24a** and **25a**, n = 1; **25b** and **26**, n = 3). These K_i values are consistent with estimated K_i values from an independent single concentration competition binding with four replicates.
[c] K_{rel}, a ratio of the K_i for the test compound to that of epibatidine from the same assay.
[d] The K_i value is adopted from[19] and the binding assay has been performed under different conditions using rat brain tissue with [^{125}I]5-A-85380 as a radioprobe.

2.5.1. Rodent studies

In the mouse study with [^{11}C]**25a**, brain radioactivity displayed regional distribution that was consistent with the known distribution of α4β2-nAChRs.[34] Brain uptake was highest in the thalamus and lowest in the cerebellum (Fig. 3). The maximal thalamus/cerebellum ratio peaked at 45 min post-injection to a value of 3.8.

The promising preliminary brain distribution data in mice suggested a necessity for more comprehensive microPET imaging studies. MicroPET experiments with [^{11}C]**25a** demonstrated excellent imaging properties of the radioligand in the rat brain (Figs. 4 and 5) with very high uptake of radioactivity in the nAChR-rich thalamus and cortical regions and low accumulation of radioactivity in the nAChR-poor cerebellum. Compounds [^{11}C]**16** and [^{11}C]**26** demonstrated a similar distribution pattern in the rat brain (Figs. 6 and 7).

Blocking studies with [^{11}C]**25a** and [^{11}C]**16** were performed by injection of cytisine, a selective α4β2-nAChR agonist. The study showed a dramatic reduction of the regional radioactivity uptake in the rat thalamus, whereas little displacement of radioactivity from the rat cerebellum was observed (Figs. 5 and 6) suggesting that in vivo binding of [^{11}C]**25a** and [^{11}C]**16** is specifically mediated by nAChR.

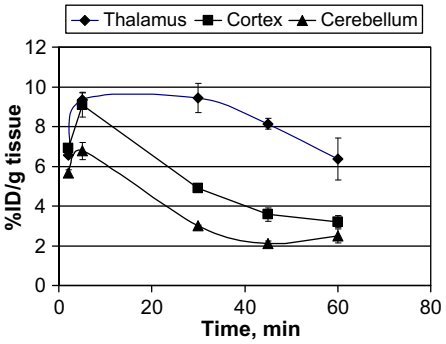

Figure 3. Regional brain time-uptake curves of [^{11}C]**25a** in mice, mean ± SD (0.07 mCi per animal, S.A. = 4900 mCi/μmol).

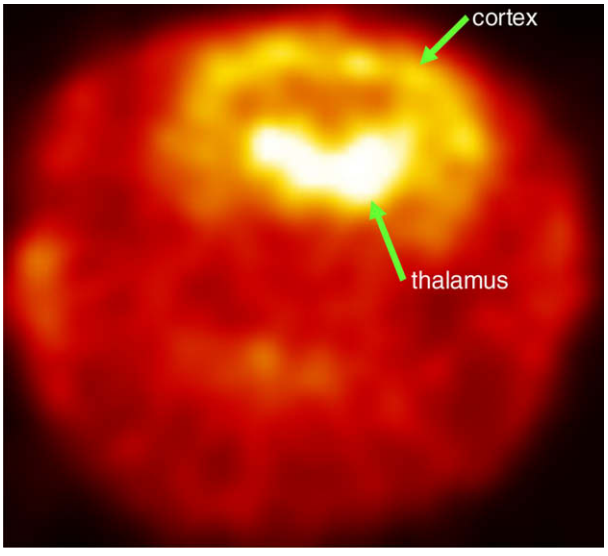

Figure 4. Small animal PET study with [^{11}C]**25a**. Summed (20–90 min) image of [^{11}C]**25a** (0.4 mCi, specific radioactivity = 4500 mCi/μmol) in a male Wistar rat (weight 153 g).

2.6. Baboon PET studies

Based on the promising results from the rodent experiments with [^{11}C]**16**, [^{11}C]**25a** and [^{11}C]**26**, PET studies in baboons were performed. All three compounds exhibited rapid accumulation of radioactivity in the baboon brain with rapid washout from the cerebellum and slow washout from the thalamus during first 90 min after injection (Figs. 8–10). The thalamus-to-cerebellum radioactivity ratios increased and approached a plateau in 90–120 min post injection (Figs. 8–10) suggesting that [^{11}C]**16**, [^{11}C]**25a** and [^{11}C]**26** manifest faster brain kinetics than has been found for **5**. PET modeling demonstrated comparable thalamic binding potential values (BP^{Th} = 0.7–0.8) of all three radioligands ([^{11}C]**16**, [^{11}C]**25a** and [^{11}C]**26**) and lower than that of **5** (Fig. 11).

The blood metabolite analysis of the radioligands [^{11}C]**16**, [^{11}C]**25a** and [^{11}C]**26** revealed substantial amounts of unidentified radiolabeled metabolites with greater retention time on the reverse-phase HPLC chromatogram (Fig. 12) that are likely to be lipophilic and, perhaps, penetrate BBB. Nonspecific binding of the lipophilic radiometabolites could be a reason of the relatively high non-specific binding and modest BP values of [^{11}C]**16**, [^{11}C]**25a** and [^{11}C]**26**.

3. Conclusion

Two new α4β2-nAChR ligands, [^{11}C]**16** and [^{11}C]**25a** have been synthesized and radiolabeled. These two radioligands and our recently developed radioligand [^{11}C]**26**,[30] have been evaluated in rats and nonhuman primates in this study. Competition binding assay with cell lines stably expressing various nAChR subtypes demonstrated that they have high affinities for β2-containing nAChR subtypes, which are predominate in the CNS. Regional brain distribution studies in rodents showed high specific accumulation of [^{11}C]**16**, [^{11}C]**25a** and [^{11}C]**26** in the nAChR-rich regions. PET imaging studies in baboons demonstrated that [^{11}C]**16**, [^{11}C]**25a** and [^{11}C]**26** label central nAChRs and the baboon brain kinetics of all three radioligands are sufficiently rapid for quantification of 120 min images. Despite the high binding affinities of [^{11}C]**16**, [^{11}C]**25a** and [^{11}C]**26** their thalamic binding potential values in baboons are lower than that of compound **5**, perhaps, due to formation of radiolabeled lipophilic metabolites.

4. Experimental

Chemicals were obtained from Aldrich (Milwaukee, WI) and used as received. Column chromatography was carried out using E. Merck silica gel 60F (230–400 mesh). Analytical thin-layer chromatography (TLC) was performed on aluminum sheets coated with Silica Gel 60 F_{254} (0.25 mm thickness, E. Merck, Darmstadt, Germany). Melting points were determined with a Fisher-Johns apparatus and are not corrected. ^{1}H NMR spectra were recorded with a Varian-400 NMR spectrometer at nominal resonance frequencies of 400 MHz in $CDCl_3$ or DMSO-d_6 (referenced to internal Me_4Si at δ_H 0 ppm). The chemical shifts (δ) were expressed in parts per million (ppm). First order J values were given in hertz. High resolution mass spectrometry was performed at the University of Notre Dame Mass Spectrometry facility. Elemental analyses were determined by Galbraith Laboratories, Inc. (Knoxville, TN). The HPLC system consisted of two Waters model 590EF pumps, two Rheodyne model 7126 injectors, an in-line Waters model 441 UV detector (254 nm) and a single sodium iodide crystal flow radioactivity detector. All HPLC chromatograms were recorded with Varian Galaxie software (version 1.8). The analytical and semi-preparative chromatography were performed using Phenomenex Luna C-18 10 μm columns (analytical 4.6 × 250 mm and semi-preparative 10 × 250 mm). A dose calibrator (Capintec 15R) was used for all

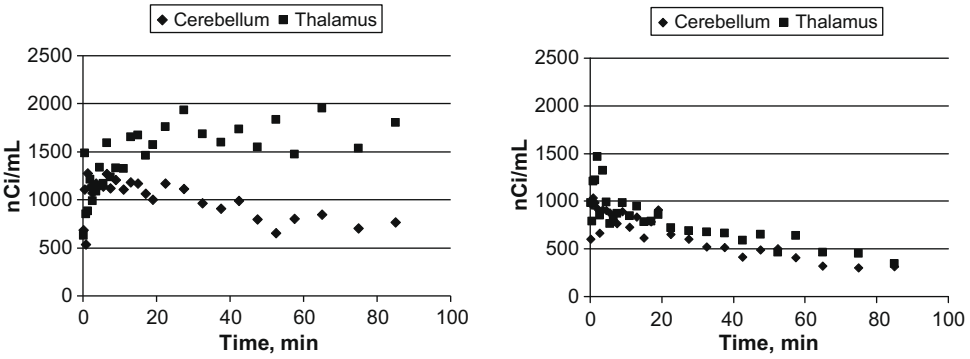

Figure 5. Time–radioactivity curves in thalamus and cerebellum of PET studies with [^{11}C]**25a** in a male Wistar rat (weight 150 g). Left panel: Time-uptake curves of [^{11}C]**25a** in the rat brain regions. Right panel: blockade study of [^{11}C]**25a** (0.4 mCi, specific radioactivity = 4000 mCi/μmol) with cytisine (2 mg/kg, iv, 5 min prior the radioligand injection).

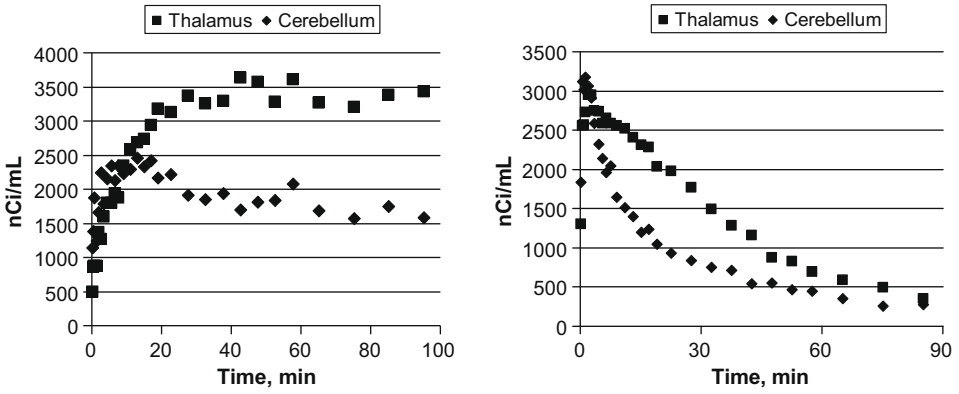

Figure 6. Time–radioactivity curves in thalamus and cerebellum of microPET studies with [^{11}C]**16** in a male Wistar rat (weight 360 g). Left panel: Baseline study with [^{11}C]**16** (0.4 mCi, specific radioactivity = 5500 mCi/μmol) Right panel: blockade study of [^{11}C]**16** (0.4 mCi, specific radioactivity = 3500 mCi/μmol) with cytisine (3 mg/kg, ip).

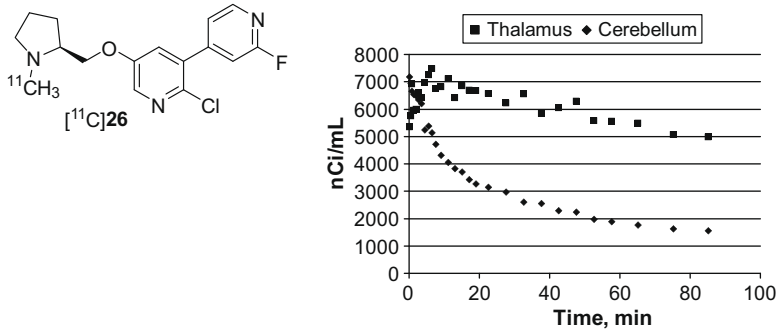

Figure 7. Time–radioactivity curves in thalamus and cerebellum of microPET study with [^{11}C]**26** in a male Wistar rat (weight 300 g). Baseline study with [^{11}C]**26** (0.6 mCi, specific radioactivity = 8200 mCi/μmol).

radioactivity measurements. [^{11}C]Methyl iodide was prepared using a General Electric Methyl Iodide Microlab from [^{11}C]carbon dioxide produced by a General Electric PETtrace biomedical cyclotron.

4.1. 3-((2-Fluoropyridin-4-yl)methoxy)pyridin-2-ol (8)

2,3-Dihydroxypyridine (0.556 g, 5 mmol) was added portionwise to a solution of NaOH (0.22 g, 5 mmol) in methanol (5 mL) followed by addition of a solution of 4-(bromomethyl)-2-fluoropyridine (0.95 g, 5 mmol) in MeOH (2 mL) dropwise during 10 min. The mixture was stirred at room temperature for 36 h. After evaporation of methanol, the residue was diluted with water (20 mL) and extracted with $CHCl_3$ (6 × 30 mL). The combined organic extracts were dried over $MgSO_4$, filtered and concentrated in vacuo. Recrystallization in ethyl acetate produced a white solid (0.89 g, 81%); mp 216–217 °C; ^{1}H NMR (400 MHz, DMSO-d_6/TMS) δ 11.72 (s, 1H), 8.26 (d, J = 5.2 Hz, 1H), 7.39 (m, 1H), 7.20 (s, 1H), 7.00 (dd, J = 1.6 Hz, 6.8 Hz, 1H), 6.92 (dd, J = 1.6 Hz, 8.0 Hz, 1H), 6.10 (t, J = 6.4 Hz, 13.6 Hz, 1H), 5.17 (s, 2H); HRMS calcd for $C_{11}H_{10}FN_2O_2$: [M+H] m/z = 221.0726, found: 221.0721.

4.2. 3-((2-Fluoropyridin-4-yl)methoxy)-5-nitropyridin-2-ol (9)

The compound **8** (440 mg, 2 mmol) was carefully dissolved in chilled H_2SO_4 (96%, 1.5 mL) and a mixture of HNO_3 (70%) /H_2SO_4 (96%) (0.2 mL of each) was added dropwise at 0–5 °C. The reaction mixture was stirred at 0–5 °C for 20 min and poured into 20 g

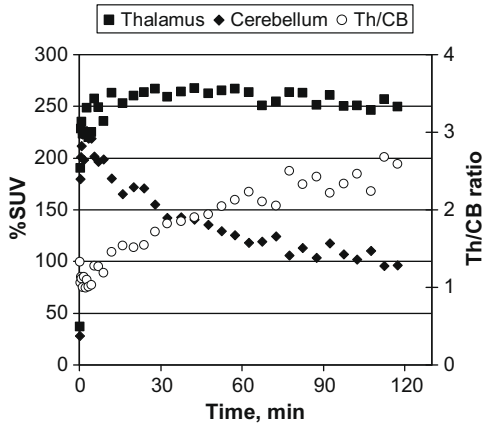

Figure 8. Time profiles of radioactivity concentrations in the baboon thalamus and cerebellum (left axis), and thalamus-to-cerebellum ratios (right axis) of [^{11}C]**25a**.

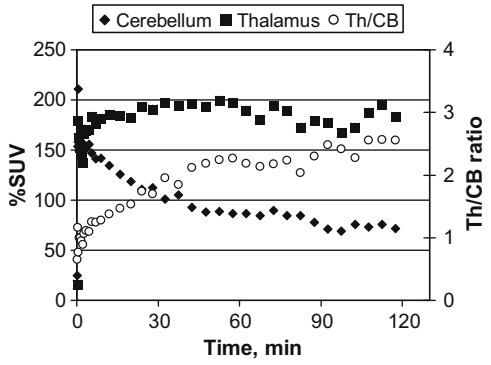

Figure 9. Thalamus and cerebellum time-uptake curves and thalamus/cerebellum ratio of accumulated radioactivity versus time in the baseline PET experiments with [^{11}C]**16** in baboon.

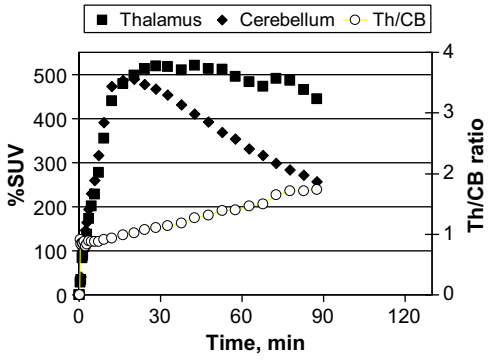

Figure 10. Thalamus/cerebellum ratio of accumulated radioactivity (%SUV = %standardized uptake value) versus time in the baseline PET experiments with [^{11}C](−)-**26** (JHU85270) in baboon.

crashed ice. The yellow precipitate was filtered off, washed with cold water (5 × 5 mL) and dried (382 mg, 72%); mp 229–230 °C; ^{1}H NMR (400 MHz, DMSO-d_6/TMS) δ 12.82 (s, 1H), 8.40 (d, J = 2.8 Hz, 1H), 8.29 (d, J = 5.2 Hz, 1H), 7.54 (d, J = 2.8 Hz, 1H), 7.42 (d, J = 5.2 Hz, 1H), 7.22 (s, 1H), 5.31 (s, 2H); HRMS calcd for $C_{11}H_9FN_3O_4$: [M+H] m/z = 266.0577, found: 266.0579.

4.3. 2-Chloro-3-(2-fluoro-4-(pyridinyl)methoxy)-5-nitropyridine (10)

Phosphoryl chloride (0.45 mL, 4.86 mmol) was added dropwise to a magnetically stirred mixture of **9** (318 mg, 1.2 mmol) and

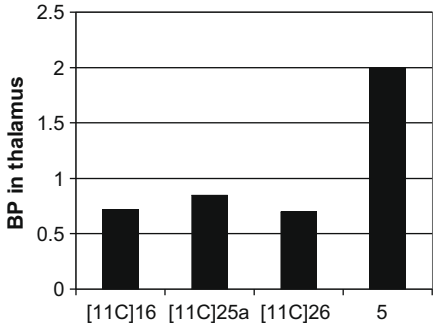

Figure 11. Histogram of binding potential estimates in the thalamus of **5** (Rhesus monkey)[35] and [^{11}C]**16**, [^{11}C]**25a** and [^{11}C]**26** (baboon).

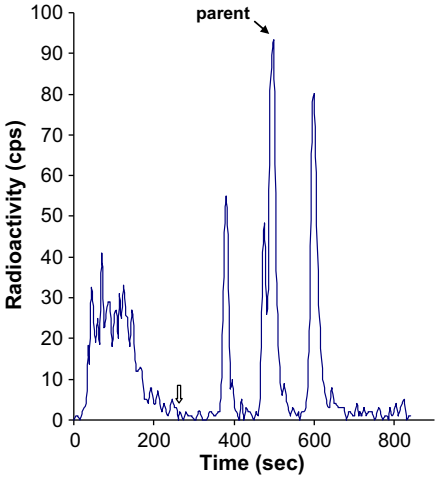

Figure 12. HPLC analysis of baboon plasma at 1 h post administration of [^{11}C]**16**. Radioligands [^{11}C]**25a** and [^{11}C]**26** exhibit similar metabolic HPLC profile.

quinoline (0.15 mL, 1.2 mmol). The mixture was blanketed with argon and heated at 120 °C for 2 h. Upon the complete consumption of the precursor, as indicated by TLC, the mixture was cooled in the ice bath and diluted with 20 mL of H_2O. The resulting brown precipitate was filtered and recrystallized from ethanol to yield sand-colored crystals (289 mg, 85%); mp 121–122 °C; ^{1}H NMR (400 MHz, $CDCl_3$/TMS) δ 8.93 (d, J = 2.4 Hz, 1H), 8.32 (d, J = 4.8 Hz, 1H), 8.01 (d, J = 2.4 Hz, 1H), 7.32 (d, J = 4.0 Hz, 1H), 7.12 (d, J = 0.8 Hz, 1H), 5.33 (s, 2H); HRMS calcd for $C_{11}H_8FN_3O_3$: [M+H] m/z = 284.0238, found: 284.0240.

4.4. 6-Chloro-5-((2-fluoropyridin-4-yl)methoxy)pyridin-3-amine (11)

The precursor **10** (490 mg, 1.72 mmol) was added to a mixture of water (5.1 mL) and glacial acetic acid (6.8 mL). Iron powder (407 mg, 7.3 mmol) was then added to the reaction flask, and the mixture was heated to 60 °C for 1 h. TLC analysis of the reaction mixture indicated a complete consumption of the precursor. Water (15 mL) was added to the reaction flask, the mixture was neutralized with potassium hydroxide pellets to pH 8 and extracted with ethyl acetate (3 × 40 mL). The ethyl acetate layer was evaporated to yield yellow solid (358 mg, 82%); mp 145–147 °C; ^{1}H NMR (400 MHz, $CDCl_3$/TMS) δ 8.26 (d, J = 5.2 Hz, 1H), 7.56 (d, J = 2.4 Hz, 1H), 7.29 (m, 1H), 7.08 (s, 1H), 6.56 (d, J = 2.0 Hz, 1H), 5.15 (s, 2H). 3.79 (br s, 2H); HRMS calcd for $C_{11}H_{10}ClFN_3O$: [M+H] m/z = 254.0496, found: 254.0498.

4.5. 6-Chloro-5-((2-fluoropyridin-4-yl)methoxy)pyridin-3-yl acetate (12)

Compound **11** (305 mg, 1.2 mmol) was added to HBF_4 (2.4 mL, 48%) at 0 °C. A solution of sodium nitrite (126 mg, 1.8 mmol) in water (0.9 mL) was added dropwise over a period of 20 min and the mixture was stirred for 1 h at 0 °C. The resulting solid was filtered, washed with cold diethyl ether (3 × 5 mL), and air-dried for 15 min. The solid was then dissolved in acetic anhydride (5 mL) and heated for 1 h to 85 °C. The solvent was evaporated, and the resulting residue was dissolved in diethyl ether (35 mL). The diethyl ether solution was washed with H_2O (2 × 20 mL), dried over $MgSO_4$, and evaporated under reduced pressure to give a residue which was purified by silica gel chromatography (hexanes/ethyl acetate 1:1). The product was obtained as white solid (230 mg, 65%); mp 102–103 °C; ^{1}H NMR (400 MHz, $CDCl_3$/TMS) δ 8.28 (d, J = 4.8 Hz, 1H), 7.93 (d, J = 2.4 Hz, 1H), 7.28 (m, 1H), 7.12 (d, J = 2.4 Hz, 1H), 7.08 (s, 1H), 5.18 (s, 2H), 2.34 (s, 3H); HRMS calcd for $C_{13}H_{11}ClFN_2O_3$: [M+H] m/z = 297.0442, found: 297.0431.

4.6. 2-Chloro-3-(2-fluoro-4-(pyridinyl)methoxy)-5-hydoxypyridine (13)

6-Chloro-5-((2-fluoropyridin-4-yl)methoxy)pyridin-3-yl acetate **12** (0.59 g, 1.99 mmol) was added to a mixture of KOH (4 mL, 1 M) and MeOH (4 mL) at 5 °C. After it was stirred for 1 h in an ice bath, TLC showed the starting material completely consumed. The solution was made acidic (pH 5), with glacial acetic acid and the resulting solid was filtered and dried. Compound **13** was obtained as a white powder (0.43 g, 85%); mp 187–188 °C; ^{1}H NMR (400 MHz, DMSO-d_6/TMS) δ 10.34 (s, 1H), 8.29 (d, J = 5.2 Hz, 1H), 8.29 (d, J = 2.8 Hz, 1H), 7.58 (d, J = 2.4 Hz, 1H), 7.41 (d, J = 5.2 Hz, 1H), 7.21 (s, 1H), 7.02 (d, J = 2.4 Hz, 1H), 5.35 (s, 2H); HRMS calcd for $C_{11}H_9Cl_2N_2O_2$: [M+H] m/z = 255.0336, found: 255.0349.

4.7. 2-Chloro-5-((1-(*tert*-butoxycarbonyl)-2-(*S*)-pyrrolidinyl)-methoxy)-3-(2-fluoro-4-(pyridinyl)methoxy)pyridine (14)

Diethyl azodicarboxylate (0.365 mL, 2.03 mmol) and triphenylphosphine (535 mg, 2.03 mmol) were mixed in THF (10 mL) at 0 °C, under argon for 30 min. *N*-Boc-L-prolinol (409 mg, 2.03 mmol) and compound **13** (398 mg, 1.56 mmol) were then added to the reaction flask, and the mixture was stirred at room temperature for 36 h. The solvent was evaporated under reduced pressure at 55 °C, and the crude oil was purified via flash chromatography (hexane/ethyl acetate 2:1–1:1). Compound **14** was obtained as colorless oil (478 mg, 70%); ^{1}H NMR (400 MHz, $CDCl_3$/TMS) δ 8.26 (m, 1H), 7.75 (d, J = 2.4 Hz, 1H), 7.42 (s, 1H), 7.29 (m, 1H), 7.08 (m, 1H), 5.29 (s, 1H), 5.17 (s, 1H), 4.25 (m, 1H), 4.06–4.12 (m, 1H), 3.90 (m, 1H), 3.29–3.49 (m, 2H), 1.91–2.06 (m, 4H), 1.48 (s, 9H); HRMS calcd for $C_{21}H_{26}ClFN_3O_4$: [M+H] m/z = 438.1596, found: 438.1587.

4.8. 2-Chloro-3-(2-fluoro-4-(pyridinyl)methoxy)-5-(2-(*S*)-pyrrolidinyl)methoxy)-pyridine (15)

TFA (2 mL) was added to a solution of the precursor **14** (370 mg, 0.84 mmol) in CH_2Cl_2 (3 mL) at 0 °C. The mixture was stirred at 0–5 °C for 2 h until the completion of the reaction, as monitored by TLC, the solvent was evaporated via rotary evaporation at 50 °C. Compound **15** was obtained via flash chromatography on a short silica gel column ($CHCl_3$/MeOH 6:1–3:1) as colorless oil (TFA salt, 820 mg, 76%). ^{1}H NMR (400 MHz, CD_3OD) δ 8.23 (d, J = 5.6 Hz, 1H), 7.77 (d, J = 2.4 Hz, 1H), 7.43 (d, J = 5.2 Hz, 1H), 7.28 (d, J = 2.0 Hz, 1H), 7.21 (s, 1H), 5.36 (s, 2H), 4.34 (m, 1H), 4.17 (m, 1H), 3.90 (m, 1H), 3.26–3.31 (m, 2H), 1.82–2.24 (m, 4H); HRMS calcd for $C_{16}H_{18}ClFN_3O_2$: [M+H] m/z = 338.1071, found: 338.1058. Anal. Calcd for $C_{16}H_{17}ClFN_3O_2 \cdot 8TFA \cdot H_2O$: C, 30.29; H, 2.15; N, 3.31. Found: C, 30.16; H, 2.19; N, 3.61.

4.9. 2-Chloro-3-(2-fluoro-4-(pyridinyl)methoxy)-5-((1-methyl-2-(*S*)-pyrrolidinyl)methoxy)pyridine (16)

A mixture of the secondary amine **15** (170 mg, 0.5 mmol) and 37% formaldehyde (0.20 mL) in acetonitrile (2 mL) was stirred for 20 min at room temperature, then sodium cyanoborohydride (50 mg, 0.8 mmol) was added in small portions. After stirring for 15 min at room temperature, acetic acid was carefully added until the solution tested neutral on wet pH paper. Stirring was continued for 2 h, HOAc being added occasionally to maintain the pH near neutrality. The solvent was evaporated at reduced pressure, and 15 mL of 5% K_2CO_3 was added to the residue. The resulting mixture was extracted with three 20 mL portions of $CHCl_3$. The combined $CHCl_3$ extracts were washed with water 10 mL, dried with anhydrous Na_2SO_4 and evaporated in vacuo to give a residue. After purification by column chromatography on silica gel with $CHCl_3$/MeOH (15:1), the product was obtained as a white solid (146 mg, 83%); ^{1}H NMR (400 MHz, $CDCl_3$/TMS) δ 8.26 (d, J = 5.2 Hz, 1H), 7.75 (d, J = 2.8 Hz, 1H), 7.28 (m, 1H), 7.08 (s, 1H), 6.84 (d, J = 2.8 Hz, 1H), 5.16 (s, 2H), 3.92–4.02 (m, 2H), 3.13 (m, 1H), 2.65 (m, 1H), 2.47 (s, 3H), 2.33 (m, 1H), 1.70–2.06 (m, 4H). Anal. Calcd for $C_{17}H_{19}ClFN_3O_2 \cdot 0.25 \cdot H_2O$: C, 57.29; H, 5.52; N, 11.80. Found: C, 57.53; H, 5.67; N, 11.82.

4.10. 3-((6-Chloropyridin-3-yl)methoxy)pyridin-2-ol (17)

2,3-Dihydroxypyridine (5.56 g, 50 mmol) was added portionwise to a solution of NaOH (2 g, 50 mmol) in methanol (30 ml), followed by addition of a solution of 2-chloro-5-(chloromethyl)pyridine (8.1 g, 50 mmol) in MeOH (10 mL) dropwise during 30 min. The mixture was stirred at room temperature for 96 h, and then heated at 40 °C for 13 h. After evaporation of methanol, the residue was diluted with water and extracted with $CHCl_3$ (6 × 100 mL). The combined organic extracts were dried over $MgSO_4$, filtered and concentrated in vacuo. Recrystallization in ethyl acetate afforded **17** (9.2 g, 78%) as white solid; mp 201–202 °C; ^{1}H NMR (400 MHz, $CDCl_3$/TMS) δ 13.00 (s, 1H), 8.46 (d, J = 2.4 Hz, 1H), 7.81 (d, J = 2.4 Hz, 1H), 7.36 (d, J = 8.4 Hz, 1H), 7.08 (dd, J = 1.6 Hz, 6.4 Hz, 1H), 6.82 (dd, J = 1.6 Hz, 6.4 Hz, 1H), 6.20 (t, J = 7.0 Hz and 14.0 Hz), 5.14 (s, 2H). HRMS calcd for $C_{11}H_{10}ClN_2O_2$: [M+H] m/z = 237.0431, found: 237.0452.

4.11. 3-((6-Chloropyridin-3-yl)methoxy)-5-nitropyridin-2-ol (18)

Compound **17** (4.8 g, 20.3 mmol) was added to magnetically stirred H_2SO_4 (96%, 15 mL) chilled with an ice-bath. Then, a cold mixture of HNO_3/H_2SO_4 (2 mL + 2 mL) was added dropwise during 20 min. The resulting mixture was stirred at 0–5 °C for 25 min and poured into 150 mL of icy water. The yellow precipitate was filtered off, washed with cold water (5 × 60 mL) and dried (4.57 g, 80%); mp 211–212 °C; ^{1}H NMR (400 MHz, DMSO-d_6/TMS) δ 12.77 (s, 1H), 8.51 (s, 1H), 8.38 (m, 1H), 7.95 (dd, J = 2.4 Hz, 8.4 Hz, 1H), 7.60 (m, 2H), 5.21 (s, 2H); HRMS calcd for $C_{11}H_9ClN_3O_4$: [M+H] m/z = 282.0282, found: 282.0276.

4.12. 2-Chloro-3-(2-chloro-5-(pyridinyl)methoxy)-5-nitropyridine (19)

Compound **18** (5.49 g, 19.5 mmol) was added to quinoline (2.35 mL, 19.6 mmol). The reaction flask was cooled to 5 °C, and phosphoryl chloride (7.3 mL, 78 mmol) was added dropwise. The mixture was blanketed with argon and heated at 120 °C for 2 h. Upon complete consumption of the precursor, as indicated by TLC, the mixture was cooled to room temperature and 100 mL of

H_2O was added. The mixture was then cooled to 0 °C and the resulting brown solid was filtered. Re-crystallization from ethanol gave sand-colored crystals, (5.22 g, 89%); mp 151–152 °C; ^{1}H NMR (400 MHz, $CDCl_3$/TMS) δ 8.92 (d, J = 2.4 Hz, 1H), 8.55 (d, J = 2.0 Hz, 1H), 8.04 (d, J = 2.4 Hz, 1H), 7.84 (dd, J = 2.4 Hz, 8.0 Hz, 1H), 7.45 (d, J = 8.4 Hz, 1H), 5.26 (s, 2H); HRMS calcd for $C_{11}H_8Cl_2N_3O_3$: [M+H] m/z = 299.9943, found: 299.9938.

4.13. 5-Amino-2-chloro-3-(2-chloro-5-(pyridinyl)methoxy)-pyridine (20)

Compound **19** (5.19 g, 17.3 mmol) was added to a solution of H_2O (51 mL) and glacial acetic acid (68 mL). Iron powder (4.06 g, 72.9 mmol) was then added to the reaction flask, and the mixture was heated to 60 °C. After 1 h, TLC monitoring of the reaction indicated complete consumption of the precursor. H_2O (100 mL) was added to the reaction flask, and the mixture was made basic, pH >8, with potassium hydroxide pellets. The mixture was then extracted with ethyl acetate (3 × 50 mL) and evaporated to a yellow solid (3.97 g, 85%); mp 152–153 °C; ^{1}H NMR (400 MHz, $CDCl_3$/TMS) δ 8.46 (d, J = 1.6 Hz, 1H), 7.82 (dd, J = 2.2 Hz, 8.2 Hz, 1H), 7.53 (d, J = 2.4 Hz, 1H), 7.39 (d, J = 8.0 Hz, 1H), 6.59 (d, J = 2.0 Hz, 1H), 5.09 (s, 2H), 3.76 (br s, 2H); HRMS calcd for $C_{11}H_{10}Cl_2N_3O$: [M+H] m/z = 270.0210, found: 270.0183.

4.14. 5-Acetyloxy-2-chloro-3-(2-chloro-5-(pyridinyl)methoxy)-pyridine (21)

Amine **20** (3.1 g, 11.5 mmol) was added to HBF_4 (24 mL, 48%) and cooled to 0 °C. A solution of sodium nitrite (1.21 g, 17.5 mmol) and H_2O (9 mL) was added dropwise over a period of 1 h. After the addition of sodium nitrite was complete, the mixture was stirred for 1 h at 0 °C. The resulting solid was filtered, washed with cold diethyl ether (3 × 20 mL), and air-dried for 15 min. The solid was then dissolved in acetic anhydride (47 mL) and heated for 1 h to 70–85 °C. The solvent was evaporated, and the resulting residue was dissolved in diethyl ether (60 mL). The diethyl ether solution was washed with H_2O (2 × 20 mL), dried over $MgSO_4$, and evaporated under reduced pressure to give a residue which was purified by silica gel chromatography (hexanes/ethyl acetate 1:1). Compound **21** was obtained as white solid (2.34 g, 72%); mp 134–135 °C; ^{1}H NMR (400 MHz, $CDCl_3$/TMS) δ 8.48 (d, J = 2.0 Hz, 1H), 7.92 (d, J = 2.0 Hz, 1H), 7.81 (dd, J = 2.4 Hz, 8.4 Hz, 1H), 7.42 (d, J = 8.0 Hz, 1H), 7.16 (d, J = 2.0 Hz, 1H), 5.13 (s, 2H), 2.34 (s, 3H); HRMS calcd for $C_{13}H_{11}Cl_2N_2O_3$: [M+H] m/z = 313.0147, found: 313.0161.

4.15. 2-Chloro-3-(2-chloro-5-(pyridinyl)methoxy)-5-hydroxypyridine (22)

Compound **21** (1.22 g, 3.9 mmol) was added to a mixture of 1 M KOH solution (6.3 mL) and MeOH (10 mL) at 5 °C. After it was stirred for 2 h in an ice bath, TLC showed the starting material completely consumed. The solution was made acidic to pH 5, with glacial acetic acid (~1.5 mL) and the resulting solid was filtered and dried. The product was obtained as a white powder (0.87 g, 82%); mp 228–229 °C; ^{1}H NMR (400 MHz, DMSO-d_6/TMS) δ 10.32 (s, 1H), 8.53 (d, J = 2.0 Hz, 1H), 7.95 (dd, J = 2.4 Hz, 8.0 Hz, 1H), 7.60 (d, J = 8.4 Hz, 1H), 7.57 (d, J = 2.4 Hz, 1H), 7.09 (d, J = 2.8 Hz, 1H), 5.26 (s, 2H); HRMS calcd for $C_{11}H_9Cl_2N_2O_2$: [M+H] m/z = 271.0041, found: 271.0024.

4.16. 2-Chloro-5-((1-(*tert*-butoxycarbonyl)-2-(*S*)-pyrrolidinyl)-methoxy)-3-(2-chloro-5-(pyridinyl)methoxy)pyridine (23a)

Diethyl azodicarboxylate (0.105 mL, 0.6 mmol) and triphenylphosphine (158 mg, 0.6 mmol) were mixed in anhydrous THF (2 mL) at 0 °C, under argon for 30 min. *N*-Boc-L-prolinol (121 mg, 0.6 mmol) and precursor **22** (121 mg, 0.45 mmol) were then added to the reaction flask, and the mixture was stirred at room temperature for 24 h. The solvent was evaporated under reduced pressure at 55 °C, and the crude oil was purified via flash chromatography (hexane/ethyl acetate 2:1–1:1). Compound **23a** was obtained as colorless oil (112 mg, 55%); ^{1}H NMR (400 MHz, $CDCl_3$/TMS) δ 8.51 (s, 1H), 7.86 (d, J = 8.0 Hz, 1H), 7.74 (d, J = 2.4 Hz, 1H), 7.47 (s, 1H), 7.39 (m, 1H), 5.25 (s, 2H), 4.24 (m, 1H), 4.09 (m, 1H), 3.88 (m, 1H), 3.39 (m, 2H), 1.88–2.00 (m, 4H), 1.48 (s, 9H); HRMS calcd for $C_{21}H_{26}Cl_2N_3O_4$: [M+H] m/z = 454.1300, found: 454.1299.

4.17. 2-Chloro-5-(1-(*tert*-butoxycarbonyl)-2-(*R*)-pyrrolidinyl)-methoxy)-3-(2-chloro-5-(pyridinyl)methoxy)pyridine (23b)

Diethyl azodicarboxylate (0.21 mL, 1.2 mmol) and triphenylphosphine (316 mg, 1.2 mmol) were mixed in anhydrous THF (5 mL) at 0 °C, under argon for 30 min. *N*-Boc-D-prolinol (242 mg, 1.2 mmol) and precursor **22** (296 mg, 1.1 mmol) were then added to the reaction flask, and the mixture was stirred at room temperature for 36 h. The solvent was evaporated under reduced pressure at 55 °C, and the crude oil was purified via flash chromatography (hexane/ethyl acetate 2:1–1:1). Compound **23b** was obtained as colorless oil (340 mg, 68%); ^{1}H NMR (400 MHz, $CDCl_3$/TMS) δ 8.51 (s, 1H), 7.86 (d, J = 8.0 Hz, 1H), 7.74 (d, J = 2.4 Hz, 1H), 7.47 (s, 1H), 7.39 (d, J = 8.4 Hz, 1H), 5.25 (s, 2H), 4.24 (m, 1H), 4.09 (m, 1H), 3.88 (m, 1H), 3.29–3.39 (m, 2H), 1.88–2.00 (m, 4H), 1.48 (s, 9H).

4.18. 5-(((*S*)-Pyrrolidin-2-yl)methoxy)-3-((6-chloropyridin-3-yl)methoxy)-2-chloropyridine (24a)

TFA (5 mL) was added to a solution of **23a** (820 mg, 1.8 mmol) in CH_2Cl_2 (6 mL) at 0 °C. The mixture was stirred at 0–5 °C for 2 h until the completion of the reaction, as monitored by TLC, the solvent was evaporated via rotary evaporation at 50 °C. Compound **24a** was obtained via flash chromatography on a short silica gel column ($CHCl_3$/MeOH 10:1) as colorless oil (510 mg, 80%). ^{1}H NMR (400 MHz, $CDCl_3$/TMS) δ 8.48 (d, J = 2.8 Hz, 1H), 7.82 (dd, J = 2.4 Hz, 8.0 Hz, 1H), 7.73 (d, J = 2.4 Hz, 1H), 7.41 (d, J = 8.4 Hz, 1H), 6.88 (d, J = 2.8 Hz, 1H), 5.12 (s, 2H), 3.93–3.97 (m, 1H), 3.85–3.89 (m, 1H), 3.53–3.57 (m, 1H), 2.98–3.03 (m, 2H), 1.93–1.98 (m, 1H), 1.79–1.87 (m, 3H), 1.53–1.58 (m, 1H). HRMS calcd for $C_{16}H_{18}Cl_2N_3O_2$: [M+H] m/z = 354.0776, found: 354.0777. Anal. Calcd for $C_{16}H_{17}Cl_2N_3O_2 \cdot TFA \cdot 0.5H_2O$: C, 45.28; H, 4.01; N, 8.81. Found, C, 45.66; H, 4.16; N, 8.70.

4.19. 5-(((*R*)-Pyrrolidin-2-yl)methoxy)-3-((6-chloropyridin-3-yl)methoxy)-2-chloropyridine (24b)

The compound **24b** was prepared via **23b** using the procedure that is described for preparation of **24a**. The product **24b** was obtained as colorless oil. Yield: 82%. ^{1}H NMR (400 MHz, $CDCl_3$/TMS) δ 8.48 (d, J = 2.8 Hz, 1H), 7.81 (dd, J = 2.4 Hz, 8.4 Hz, 1H), 7.74 (d, J = 2.4 Hz, 1H), 7.40 (d, J = 8.0 Hz, 1H), 6.89 (d, J = 2.8 Hz, 1H), 5.12 (s, 2H), 3.95–3.98 (m, 1H), 3.87–3.91 (m, 1H), 3.53–3.58 (m, 1H), 2.98–3.04 (m, 2H), 2.09 (br s, 1H), 1.94–2.02 (m, 1H), 1.78–1.89 (m, 2H), 1.52–1.61 (m, 1H). Anal. Calcd for $C_{16}H_{17}Cl_2N_3O_2 \cdot TFA \cdot H_2O$: C, 44.53; H, 4.16; N, 8.66. Found: C, 44.36; H, 4.00; N, 8.58.

4.20. 2-Chloro-3-(2-chloro-5-(pyridinyl)methoxy)-5-((1-methyl)-2-(*S*)-pyrrolidinyl)methoxy)pyridine (25a)

Compound **24a** (145 mg, 0.32 mmol) was dissolved in a mixture of formic acid (0.35 mL) and formalin (0.7 mL), refluxed for 8 h, and cooled to room temperature. The reaction mixture was poured into

5% K_2CO_3 solution in water (20 mL). The aqueous mixture was extracted with $CHCl_3$ (4 × 15 mL), the combined extracts were washed with water (20 mL), dried over Na_2SO_4, and the solvent was removed. The residue was chromatographed on silica gel ($CHCl_3$/MeOH 15:1) to give the product as a white solid (76 mg, 65%); ^{1}H NMR (400 MHz, $CDCl_3$/TMS) δ 8.48 (d, J = 2.4 Hz, 1H), 7.82 (dd, J = 2.4 Hz, 8.8 Hz, 1H), 7.73 (d, J = 2.4 Hz, 1H), 7.40 (d, J = 8.4 Hz, 1H), 6.89 (d, J = 2.8 Hz, 1H), 5.11 (s, 2H), 3.93–4.02 (m, 2H), 3.13 (m, 1H), 2.65 (m, 1H), 2.47 (s, 3H), 2.30 (m, 1H), 2.02 (m, 1H), 1.74–1.83 (m, 3H); HRMS calcd for $C_{17}H_{20}Cl_2N_3O_2$: [M+H] m/z = 368.0933, found: 368.0929; Anal. Calcd for $C_{17}H_{19}Cl_2N_3O_2$: C, 55.45; H, 5.20; N, 11.41. Found: C, 55.30; H, 5.36; N, 11.43.

4.21. 2-Chloro-3-(2-chloro-5-(pyridinyl)methoxy)-5-((1-methyl)-2-(*R*)-pyrrolidinyl)methoxy)pyridine (25b)

This compound was prepared similar to compound **25a**. The product was obtained as white solid. Yield: 72%. ^{1}H NMR (400 MHz, $CDCl_3$/TMS) δ 8.48 (d, J = 2.0 Hz, 1H), 7.82 (dd, J = 2.4 Hz, 8.4 Hz, 1H), 7.73 (d, J = 2.4 Hz, 1H), 7.40 (d, J = 8.4 Hz, 1H), 6.89 (d, J = 2.4 Hz, 1H), 5.11 (s, 2H), 3.93–4.02 (m, 2H), 3.13 (m, 1H), 2.65 (m, 1H), 2.47 (s, 3H), 2.30 (m, 1H), 2.02 (m, 1H), 1.72–1.86 (m, 3H); HRMS calcd for $C_{17}H_{20}Cl_2N_3O_2$: [M+H] m/z = 368.0933, found: 368.0926; Anal. Calcd for $C_{17}H_{19}Cl_2N_3O_2 \cdot 0.25 \cdot H_2O$: C, 54.90; H, 5.29; N, 11.31. Found. C, 54.69; H, 5.32; N, 11.23.

5. Radiochemistry

5.1. 2-Chloro-3-(2-fluoro-4-(pyridinyl)methoxy)-5-((1-[^{11}C]-methyl-2-(*S*)-pyrrolidinyl)methoxy)pyridine ([^{11}C]16)

Precursor **15** (1–2 mg) was dissolved in 200 μL of anhydrous DMF, capped in a small V-vial and cooled to −40 °C. [^{11}C]Methyl iodide was swept by argon flow into the solution. After the radioactivity reached a plateau, the vial was assayed in the dose calibrator and then heated at 80 °C for 5 min. Water (200 μL) was added and the solution was injected onto the semi-preparative HPLC column (Phenomenex Luna C-18 10 μm column, semi-preparative 10 × 250 mm, 30:70 v/v CH_3CN/0.1 M ammonium formate, 12 mL/min). The retention time of **15** was 3.8 min. The product [^{11}C]**16** peak, having retention time of 5.2 min, was collected into a flask containing 50 mL water. The mixture was transferred through a Waters C-8 Sep-Pak Plus. The product was eluted with 1 mL ethanol into a vial and diluted with 9 mL of 0.9% saline. The final product [^{11}C]**16** was then analyzed by analytical HPLC (Phenomenex Luna C-18 10 μm columns, analytical 4.6 × 250 mm, 30:70 v/v CH_3CN/0.1 M ammonium formate, 3 mL/min, t_R = 2.5 min) to determine the radiochemical purity (>98%) and the specific radioactivity at the time of synthesis. The total synthesis time was 35 min from EOB with an average radiochemical yield of 18.4 ± 8.8% and specific radioactivity of 8022 ± 5592 (n = 4) mCi/μmol (nondecay corrected from the end of $^{11}CH_3I$ synthesis).

5.2. 2-Chloro-3-(2-chloro-5-(pyridinyl)methoxy)-5-((1-[^{11}C]methyl)-2-(*S*)-pyrrolidinyl)methoxy)pyridine ([^{11}C]25a)

Precursor **24a** (1.5 mg) was dissolved in 200 μL of anhydrous DMF, capped in a small V-vial and cooled to −40 °C. [^{11}C]Methyl iodide was swept by argon flow into the vial. After the radioactivity reached a plateau, the vial was assayed in the dose calibrator and then heated at 80 °C for 5 min. Water (200 μL) was added and the solution was injected onto the semi-preparative HPLC column (Phenomenex Luna C-18 10 μm column, semi-preparative 10 × 250 mm, 32:68 v/v CH_3CN/0.1 M ammonium formate, 8 mL/min). The retention time of normethyl precursor **24a** was 4.7 min. The product peak, having retention time of 7.7 min, was collected into a flask containing 50 mL water. The water solution was transferred through a Waters C-8 Sep-Pak Plus. The product was eluted with 1 mL ethanol into a vial and diluted with 9 mL of 0.9% saline. The final product [^{11}C]**25a** was then analyzed by analytical HPLC (Phenomenex Luna C-18 10 μm columns, analytical 4.6 × 250 mm, 40:60 v/v CH_3CN/0.1 M ammonium formate, 2 mL/min, t_R = 3.5 min) to determine the radiochemical purity (>98%) and the specific radioactivity at the time of synthesis. The total synthesis time was 40 min from EOB with an average radiochemical yield of 29 ± 7.2% and specific radioactivity of 3646 ± 1233 mCi/μmol (nondecay corrected from the end of $^{11}CH_3I$ synthesis).

6. Animal studies

All animal studies were approved by the Animal Care and Use Committee of the Johns Hopkins University.

6.1. Mouse studies

Baseline Study. Male, CD-1 mice weighing 25–30 g from Charles River Laboratories, (Wilmington, MA) were used for biodistribution studies. The animals were sacrificed by cervical dislocation at 5, 15, 30 and 60 min after intravenous injection of radiotracer in 200 μL saline vehicle into a lateral tail vein (3 animals per time-point). The brains were rapidly removed and dissected on ice. The brain regions of interest were blotted, weighed and their radioactivity content was determined in an automated γ-counter with a counting error below 3%. Aliquots of the injectate were prepared as standards and their radioactivity content was counted along with the tissue samples. The percent of injected dose per gram of tissue (%ID/g tissue) was calculated. To assess binding specificity, blocking studies were performed in the same manner as described above except that 0.2 mL of a solution containing the blocking dose in saline was administered 5 min prior to subcutaneous (s.c.) injection of the radioligand.

6.2. Micro PET studies with rats

A male Wistar rat (Charles River) was anesthetized by intraperitoneal administration of a combination of ketamine (72 mg/kg), xylazine (6 mg/kg), and acepromazine (6 mg/kg) and positioned on the bed of the GE eXplore Vista small-animal PET scanner (GE Medical Systems, Waukesha, WI) and kept anesthetized with isoflurane (0.5–1%; approximately 1 L/min). The radiotracer (11.1 MBq or 0.3 mCi in 0.2 mL of saline) or blocking agent cytisine were injected via the tail vein. After the radioligand injection, the PET images were acquired using a 28 dynamic frame protocol (90 min total; 3 × 20 s, 3 × 40 s, 5 × 60 s, 6 × 120 s, 8 × 300 s, 3 × 600 s). PET images were reconstructed using a 2D OSEM algorithm after subtracting the scatter component from the sonogram images. Mean images were created and they were used for drawing regions of interest (ROIs) on the thalamus and the cerebellum. For each region the ROI was drawn on two adjacent slices, then the ROIs were applied to the dynamic images to generate time–activity curves.

6.3. Baboon PET experiments

Male baboons (*Papio anubis*) (20–26 kg) were studied in baseline control experiments. The animals were fasted for 12 h prior to the PET study. Anesthesia was given initially with intramuscular injection of 20 ml (9 mg/kg) Saffan® (Schering-Plough,

Middlesex, UK). The baboon was intubated and anesthesia was maintained with a constant infusion of Saffan® diluted with isotonic saline (1:4) at an average flow rate that corresponded to 7.5 mg/kg/h. Circulatory volume was maintained by infusion of isotonic saline. An arterial catheter was inserted for blood sampling. Physiological vital signs including heart rate, ECG, blood pressure and oxygen saturation were continuously monitored throughout the study.

The animal was positioned in a high resolution research tomograph (ECAT HRRT) brain PET scanner (CPS Innovations, Inc., Knoxville, TN). A custom thermoplastic mask was molded to the shape of the baboon head and attached to the PET scanner bed to reproducibly position the animal and restrict motion during the PET scan.

A 6 min transmission scan with a 1 mCi Germanium-68 source was initially performed for attenuation correction. Then dynamic PET data were acquired in 3D list mode during a 120 min period following a bolus injection of the radioligand ([^{11}C]**16** (21 mCi, specific radioactivity = 2900 mCi/μmol) or [^{11}C]**24a** (17.5 mCi, specific radioactivity = 2800 mCi/μmol) or ([^{11}C]**26** (31 mCi, specific radioactivity = 11,600 mCi/μmol) in a list mode. Arterial blood was sampled rapidly initially and with prolonging intervals throughout the scan.

Volumes of interest (VOIs) were defined on SPGR (spoiled gradient) MRI acquired in the Signa 1.5 Tesla scanner (GE Medical Systems, Milwaukee, WI) for thalamus and cerebellum. VOIs were transferred to PET space using MRI-to-PET coregistration parameters[36] and applied on PET frames to generate time–radioactivity curves (TACs) of the regions. Fractions of unmetabolized radio-tracers in plasma for arterial blood samples that underwent HPLC analysis were fitting with a sum of two exponentials to obtain metabolite-corrected plasma TACs. A two-tissue compartmental model with four parameters (i.e., K_1 and k_2 for blood-to brain and brain-to-blood clearance rate constants across the blood–brain-barrier, and k_3 and k_4 for association and dissociation rate constants to and from receptors) was used to describe the kinetics of radiotracers. Three parameters (K_1, k_3, and k_4) were estimated in thalamus by setting the K_1–k_2 ratio to the estimate obtained in cerebellum.[37] A fixed fraction (3.5%) of total plasma TAC was subtracted from tissue TAC at each PET frame to remove the radioactivity in vasculature in tissue. The outcome variable, binding potential was given as the k_3–k_4 ratio[38,39] The possibility that lipophilic metabolites might enter the brain was ignored in tracer kinetics modeling.

6.4. Metabolite analysis in baboon plasma

Metabolites of [^{11}C]**16**, [^{11}C]**25a** and ^{11}C]**26** in baboon were studied using a general method previously developed for PET radiotracers.[40] Specifically, arterial blood samples were withdrawn at 5, 15, 30, 60, and 90 min intervals up to 90 min post-injection and plasma was analyzed for the presence of the parent radioligands and their radiolabeled metabolites. Briefly, 3 mL of plasma in 8 M urea were passed through a capture column (19 × 4.6 mm Strata-X, Phenomenex, Torrance, CA) at 2 mL/min, followed by 1% acetonitrile in water to wash plasma proteins from the column. The effluent from the capture column, containing only highly polar components, flows through a dual BGO detector (Bioscan, Washington, DC). The solvent was then switched to a mixture of 35% acetonitrile/65% 0.1 M aqueous ammonium bicarbonate (2 mL/min) for elution of the radiolabeled components bound to the capture column onto the analytical column (Gemini C18, 4.6 × 250 mm, Phenomenex, Torrance, CA).

Acknowledgments

The authors thank Paige Finley for her help with the animal experiments, Robert C. Smoot for radiochemistry assistance, and James Fox, David J. Clough and Karen Edmonds for PET scanner operation. We are grateful to Judy W. Buchanan for editorial help. This research was supported by the Department of Radiology of Johns Hopkins University School of Medicine and U.S. Public Health Service grants from the National Institutes of Health (DA020777 and MH079017). The National Institute of Mental Health Psychoactive Drug Screening Program (Grant N01 MH32004) supported some of the in vitro studies.

References and notes

1. Le Novere, N.; Changeux, J. P. *Nucleic Acids Res.* **1999**, *27*, 340.
2. Corringer, P. J.; Le Novere, N.; Changeux, J. P. *Annu. Rev. Pharmacol. Toxicol.* **2000**, *40*, 431.
3. Karlin, A. *Nat. Rev. Neurosci.* **2002**, *3*, 102.
4. Millar, N. S. *Biochem. Soc. Trans.* **2003**, *31*, 869.
5. Clementi, F.; Fornasari, D.; Gotti, C. *Trends Pharmacol. Sci.* **2000**, *21*, 35.
6. Romanelli, M. N.; Gratteri, P.; Guandalini, L.; Martini, E.; Bonaccini, C.; Gualtieri, F. *ChemMedChem* **2007**, *2*, 746.
7. Holladay, M. W.; Dart, M. J.; Lynch, J. K. *J. Med. Chem.* **1997**, *40*, 4169.
8. Lloyd, G. K.; Williams, M. *J. Pharmacol. Exp. Ther.* **2000**, *292*, 461.
9. Abreo, M. A.; Lin, N. H.; Garvey, D. S.; Gunn, D. E.; Hettinger, A. M.; Wasicak, J. T.; Pavlik, P. A.; Martin, Y. C.; Donnelly-roberts, D. L.; Anderson, D. J.; Sullivan, J. P.; Williams, M.; Arneric, S. P.; Holladay, M. W. *J. Med. Chem.* **1996**, *39*, 817.
10. Lin, N. H.; Li, Y.; He, Y.; Holladay, M. W.; Kuntzweiler, T.; Anderson, D. J.; Campbell, J. E.; Arneric, S. P. *Bioorg. Med. Chem. Lett.* **2001**, *11*, 631.
11. Horti, A. G.; Villemagne, V. L. *Curr. Pharm. Des.* **2006**, *12*, 3877.
12. Paterson, D.; Nordberg, A. *Prog. Neurobiol.* **2000**, *61*, 75.
13. Gundisch, D. *Curr. Pharm. Des.* **2000**, *6*, 1143.
14. Villemagne, V. L.; Musachio, J. L.; Scheffel, U. In *Neuronal Nicotinic Receptors, Pharmacology and Therapeutic Opportunities*; Arneric, S. P., Brioni, J. D., Eds.; Johns Wiley & Sons: New York, 1999; p 235.
15. Sihver, W.; Langstrom, B.; Nordberg, A. *Acta Neurol. Scand. Suppl.* **2000**, *176*, 27.
16. Sihver, W.; Nordberg, A.; Langstrom, B.; Mukhin, A. G.; Koren, A. O.; Kimes, A. S.; London, E. D. *Behav. Brain Res.* **2000**, *113*, 143.
17. Volkow, N. D.; Ding, Y. S.; Fowler, J. S.; Gatley, S. J. *Biol. Psychiatry* **2001**, *49*, 211.
18. Ding, Y. S.; Fowler, J. *Nucl. Med. Biol.* **2005**, *32*, 707.
19. Kimes, A. S.; Horti, A. G.; London, E. D.; Chefer, S. I.; Contoreggi, C.; Ernst, M.; Friello, P.; Koren, A. O.; Kurian, V.; Matochik, J. A.; Pavlova, O.; Vaupel, D. B.; Mukhin, A. G. *FASEB J.* **2003**, *17*, 1331.
20. Bottlaender, M.; Valette, H.; Roumenov, D.; Dolle, F.; Coulon, C.; Ottaviani, M.; Hinnen, F.; Ricard, M. *J. Nucl. Med.* **2003**, *44*, 596.
21. Ding, Y. S.; Fowler, J. S.; Logan, J.; Wang, G. J.; Telang, F.; Garza, V.; Biegon, A.; Pareto, D.; Rooney, W.; Shea, C.; Alexoff, D.; Volkow, N. D.; Vocci, F. *Synapse* **2004**, *53*, 184.
22. Dollé, F.; Dolci, L.; Valette, H.; Hinnen, F.; Vaufrey, F.; Guenther, I.; Fuseau, C.; Coulon, C.; Bottlaender, M.; Crouzel, C. *J. Med. Chem.* **1999**, *42*, 2251.
23. Mitkovski, S.; Villemagne, V. L.; Novakovic, K. E.; O'Keefe, G.; Tochon-Danguy, H.; Mulligan, R. S.; Dickinson, K. L.; Saunder, T.; Grégoire, M.-C.; Bottlaender, M.; Dollé, F.; Rowe, C. C. *Nucl. Med. Biol.* **2005**, *32*, 585.
24. Gallezot, J.-D.; Bottlaender, M.; Grégoire, M.-C.; Roumenov, D.; Deverre, J.-R.; Coulon, C.; Ottaviani, M.; Dollé, F.; Syrota, A.; Valette, H. *J. Nucl. Med.* **2005**, *46*, 240.
25. Horti, A. G.; Chefer, S. I.; Mukhin, A. G.; Koren, A. O.; Gundisch, D.; Links, J. M.; Kurian, V.; Dannals, R. F.; London, E. D. *Life Sci.* **2000**, *67*, 463.
26. Horti, A. G.; Gao, Y.; Kuwabara, H.; Dannals, R. F. *Life Sci.* **2009**, in press. doi:10.1016/j.lfs.2009.02.029.
27. Brown, L.; Chefer, S.; Pavlova, O.; Vaupel, D. B.; Koren, A. O.; Kimes, A. S.; Horti, A. G.; Mukhin, A. G. *J. Neurochem.* **2004**, *91*, 600.
28. Brown, L. L.; Kulkarni, S.; Pavlova, O. A.; Koren, A. O.; Mukhin, A. G.; Newman, A. H.; Horti, A. G. *J. Med. Chem.* **2002**, *45*, 2841.
29. Brown, L. L.; Pavlova, O.; Mukhin, A.; Kimes, A. S.; Horti, A. G. *Bioorg. Med. Chem.* **2001**, *9*, 3055.
30. Gao, Y.; Ravert, H. T.; Holt, D.; Dannals, R. F.; Horti, A. G. *Appl. Radiat. Isot.* **2007**, *65*, 947.
31. Waterhouse, R. N. *Mol. Imaging Biol.* **2003**, *5*, 376.
32. Xiao, Y.; Kellar, K. J. *J. Pharmacol. Exp. Ther.* **2004**, *310*, 98.
33. Meyer, E. L.; Xiao, Y.; Kellar, K. J. *Mol. Pharmacol.* **2001**, *60*, 568.
34. Lukas, R. J.; Changeux, J. P.; Le Novere, N.; Albuquerque, E. X.; Balfour, D. J.; Berg, D. K.; Bertrand, D.; Chiappinelli, V. A.; Clarke, P. B.; Collins, A. C.; Dani, J. A.; Grady, S. R.; Kellar, K. J.; Lindstrom, J. M.; Marks, M. J.; Quik, M.; Taylor, P. W.; Wonnacott, S. *Pharmacol. Rev.* **1999**, *51*, 397.
35. Chefer, S. I.; London, E. D.; Koren, A. O.; Pavlova, O. A.; Kurian, V.; Kimes, A. S.; Horti, A. G.; Mukhin, A. G. *Synapse* **2003**, *48*, 25.
36. Ashburner, J. T.; Friston, K. J. In *Statistical Parametric Mapping: The Analysis of Functional Brain Images*; Friston, K. J., Ashburner, J. T., Kiebel, S. J., Nichols, T. E., Eds.; Academic Press, 2007.

37. Kuwabara, H.; Cumming, P.; Reith, J.; Leger, G.; Diksic, M.; Evans, A. C.; Gjedde, A. *J. Cereb. Blood Flow Metab.* **1993**, *13*, 43.
38. Mintun, M. A.; Raichle, M. E.; Kilbourn, M. R.; Wooten, G. F.; Welch, M. J. *Ann. Neurol.* **1984**, *15*, 217.
39. Innis, R. B.; Cunningham, V. J.; Delforge, J.; Fujita, M.; Gjedde, A.; Gunn, R. N.; Holden, J.; Houle, S.; Huang, S. C.; Ichise, M.; Iida, H.; Ito, H.; Kimura, Y.; Koeppe, R. A.; Knudsen, G. M.; Knuuti, J.; Lammertsma, A. A.; Laruelle, M.; Logan, J.; Maguire, R. P.; Mintun, M. A.; Morris, E. D.; Parsey, R.; Price, J. C.; Slifstein, M.; Sossi, V.; Suhara, T.; Votaw, J. R.; Wong, D. F.; Carson, R. E. *J. Cereb. Blood Flow Metab.* **2007**, *27*, 1533.
40. Hilton, J.; Yokoi, F.; Dannals, R. F.; Ravert, H. T.; Szabo, Z.; Wong, D. F. *Nucl. Med. Biol.* **2000**, *27*, 627.